ORIGINAL CONTRIBUTION

Bread dough rheology: an improved damage function model

Roger Ian Tanner · Fuzhong Qi · Shaocong Dai

Abstract We describe an improved damage function model for bread dough rheology. The model has relatively few parameters, all of which can easily be found from simple experiments as discussed in this paper. Small deformations in the linear region are described by a gel-like power-law memory function. Then, we consider a set of large non-reversing deformations—stress relaxation after a step of shear, steady shearing and elongation beginning from rest and biaxial stretching. With the introduction of a revised strain measure which includes a Mooney–Rivlin term, all of these motions can be well described by the damage function described previously. For reversing step strains, larger amplitude oscillatory shearing and recoil we present a discussion which shows how the damage function model can be applied in these cases.

Keywords Dough rheology · Biaxial strain · Damage function · Viscoelasticity

Introduction to the damage function concept

According to a well-known review by Bloksma (1990), dough rheology plays an important role in determining the processing behaviour and final quality of baked products. Dough is not a simple material; it is a polymeric network with about 60% by volume of starch

R. I. Tanner (✉) · F. Qi · S. Dai
School of Aerospace, Mechanical and Mechatronic
Engineering, University of Sydney, Sydney,
NSW 2006, Australia
e-mail: r.tanner@usyd.edu.au, rit@aeromech.usyd.edu.au

filler particles, and constitutive models for such materials are still being sought.

Clearly, a model should have as few parameters as possible, and these can then be studied for various mixes of dough with various breeds of wheat. Some progress towards this end has been made with a so-called damage function model (Tanner et al. 2007, 2008a), and the model has been applied to the description of JANZ dough (a hard Australian wheat), Rosella (a softer Australian wheat) and two Iranian wheat breeds (Amirkaveei et al. 2009).

Here, we suggest an improved version of the model; we draw together previously scattered results for the model and present some new results. We also indicate ways of determining the model parameters from available testing procedures.

The general form of the model relates the stress (σ) to the strain (**S**) by a viscoelastic memory integral over all past history of deformation. We write, for the stresses at time t:

$$\boldsymbol{\sigma} + P\mathbf{I} = f \int_{-\infty}^{t} m(t - t')\mathbf{S}(t')dt' \tag{1}$$

in which σ is the total stress tensor, P is the pressure, f is the damage function, m is the memory function and **S** is the strain tensor to be defined later (Eq. 7).

Here, we assume the dough is incompressible (see Wang et al. 2006 for a discussion of the bulk modulus of dough), so the pressure P (multiplied by the unit tensor **I**) has to be introduced; P must be found from the equations of motion if needed. The memory function m in Eq. 1 is a function of the difference of the prior time t' from the present time t; in this paper we assume, following earlier work (Gabriele et al. 2001; Tanner et al.

2007, 2008a; Ng and McKinley 2008; Leroy et al. 2010) that a simple gel-like power-law form is applicable:

$$m(t) = pG(1)t^{-(1+p)}. \tag{2}$$

This form contains only two parameters, p and $G(1)$. The 'damage function' f is unity for very small strains (no damage) and decreases sharply as the strain increases from zero. (In the work of Ng and McKinley (2008), it is not clear how their 'damping function' is to be used in complex flows, and in any case the idea does not seem to be equivalent to the damage function of Eq. 1).

The Finger strain measure $(\mathbf{C}^{-1}(t'))$ was used in our previous work (instead of $\mathbf{S}$). This strain measure is computed relative to the current configuration at time t which places a dough particle at $\mathbf{x}(t)$; the previous place of the particle at time t' is denoted by $\mathbf{r}(t')$. We define (Tanner 2000) the deformation gradient $\mathbf{F}$ as

$$\mathbf{F} = \frac{\partial \mathbf{r}}{\partial \mathbf{x}} \tag{3}$$

Then the Cauchy–Green strain tensor $(\mathbf{C}(t'))$ is defined as

$$\mathbf{C} = \mathbf{F}^T \mathbf{F} \tag{4}$$

where $\mathbf{F}^T$ denotes the transpose of $\mathbf{F}$. The Finger tensor is then $\mathbf{C}^{-1}$.

We shall mainly deal here with shearing and elongational/biaxial deformations. It is well-known (e.g. Tanner 2000) that, for a shear of amount γ, the $\mathbf{C}$ tensor is

$$\mathbf{C} = \begin{bmatrix} 1 & -\gamma & 0 \\ -\gamma & 1+\gamma^2 & 0 \\ 0 & 0 & 1 \end{bmatrix} \tag{5}$$

and the Finger tensor $\mathbf{C}^{-1}$ is

$$\mathbf{C}^{-1} = \begin{bmatrix} 1+\gamma^2 & \gamma & 0 \\ \gamma & 1 & 0 \\ 0 & 0 & 1 \end{bmatrix} \tag{6}$$

In the present paper we will use a strain $\mathbf{S}$ that is a linear combination of $\mathbf{C}$ and $\mathbf{C}^{-1}$, so that we define the strain $\mathbf{S}$ (Eq. 1) as

$$\mathbf{S} = \frac{1}{1+a}(\mathbf{C} - a\mathbf{C}^{-1}) \tag{7}$$

where a is a constant. We shall often be concerned with the shear stress response and so the square-law (normal stress) terms in Eqs. 5 and 6 are not used here. For a shear displacement in the x-direction the (xy) component of the strain $\mathbf{S}$ is then, from Eqs. 5–7

$$S_{xy} = \gamma \tag{8}$$

which is unchanged from the Finger tensor component used previously (Tanner et al. 2008a) regardless of the value of a.

It is desirable to test the model in a wide range of deformation patterns. We have considered:

1. Small-strain deformations;
2. Relaxation of stress after a single suddenly applied step of shear;
3. Simple shearing beginning from rest;
4. Biaxial stretching beginning from rest;
5. Constant-rate elongation beginning from rest;
6. Sequences of step strains;
7. Larger amplitude sinusoidal strains;
8. Recoil after elongation;
9. Creep.

Creep will not be discussed here; it will be treated in another paper. Of these tests, 2 to 5 and creep are non-reversing deformations, whilst 1 and 6 to 8 involve reversal of strain. We will mainly be concerned with categories b to f above. One needs to be careful in evaluating the integral in Eq. 1. For example, the case of a steady simple shear of rate $\dot{\gamma}$ s^{-1}, beginning at $t = 0$, we need to find $\gamma(t')$ for all values of t' to compute the integral in Eq. 1. There are two regions:

1. If $0 < t' < $ t then $\gamma(t') = \dot{\gamma}(t - t')$ (9)

2. If $-\infty < t' \leq 0$ then $\gamma(t') = \dot{\gamma}t$ (10)

The part of strain history in Eq. 10 must not be ignored. A further discussion of the calculation methods used is given in Appendix B.

These results follow from Eqs. 5 and 6 above. The calculation of the integral in Eq. 1 using Eqs. 9, 10 and the memory function (2) gives, for the shear stress τ (t), the result:

$$\tau = pfG(1)\dot{\gamma} \left\{ \int_0^t (t-t')^{-p}dt' + t\int_{-\infty}^0 (t-t')^{-(1+p)}dt' \right\} \tag{11}$$

The model shear stress response can be put in the form (shear rate)^p × function of shear strain:

$$\tau = \frac{f}{1-p}G(1)\dot{\gamma}t^{1-p} = \frac{f}{1-p}G(1)\dot{\gamma}^p\gamma^{1-p} \tag{12}$$

where the shear strain $\gamma = \dot{\gamma}t$, and f, the damage function, are functions of γ. (The result (12), with $f = 1$, was first given by Winter and Mours 1997.)

For other steady flows beginning from rest results similar to Eq. 12 hold (Tanner et al. 2008a). The stresses are always found to be of the form (rate of

deformation)^p times a function of strain; the explicit result for elongational flows beginning from rest has been given previously (Tanner et al. 2008a). We shall use these results to assist in finding the damage function f.
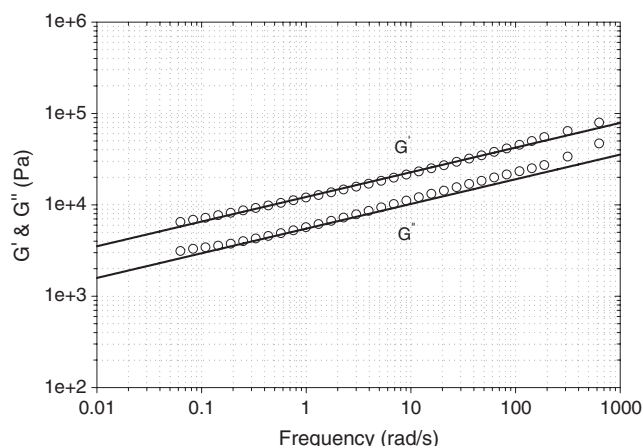
Finding the model parameters

It is important that the deduction of the parameters of the model is simple and accessible. We can proceed as follows:

1. Small strain oscillatory testing

A standard set of tests at small sinusoidal-in-time shear strains at various frequencies (ω rad/s) can be used to find p and $G(1)$ (Eq. 2). In this case, for strain amplitudes of 0.001 or less, the response of dough is linear, $f = 1$, and the shear response can be shown to be given (Pipkin 1986) by the power-law in-phase (G') and out-of-phase (G'') modulus functions. The values of G', G'' are proportional to ω^p and the slope of the logarithmic plots finds p. An example for JANZ dough is shown in Fig. 1. To find $G(1)$, we note (Pipkin 1986) that if we measure the value of $G'(\omega)$ at $\omega = 1$ rad/s, equal to $G'(1)$, then

$$G(1) = \frac{2G'(1)(p!)}{p\pi} \sin \frac{p\pi}{2} \qquad (13)$$

which enables $G(1)$ in Eq. 2 to be found (we use the notation $p!$ to denote the factorial function of p (Abramowitz and Stegun 1965): for those who prefer the gamma function notation the relation between the two is simply $z! = \Gamma(1 + z)$).

For the data of Fig. 1 (JANZ dough), we find $p \sim 0.27$, $G(1) = 10.7$ kPa s$^{0.27}$. Also, the value of G'' is then easily found; we have

$$\tan \delta = \frac{G''}{G'} = \tan \frac{p\pi}{2} \qquad (14)$$

In this case, $\tan \delta \approx 0.45$ and $G(1)/G'(1) \sim 0.88$. Since $G' > G''$, the material behaviour is solid-like. The persistence of the power-law region at high frequencies (up to 400 kHz) is surprising as has been shown by Leroy et al. (2010).
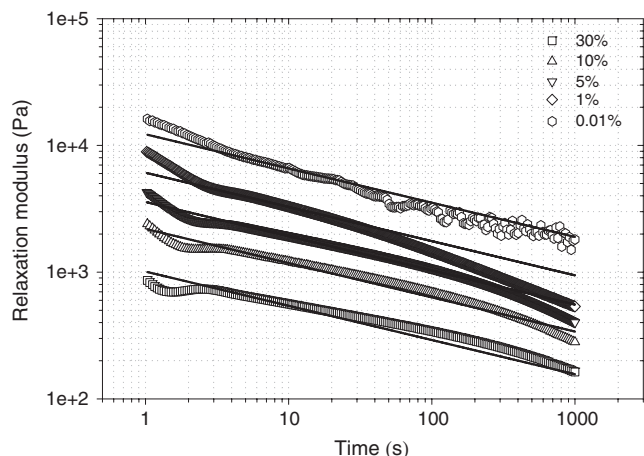
2. Stress relaxation after a step of shear

In this case, we suppose a step of shear of magnitude γ is suddenly applied at $t = 0$. The shear stress response $\tau(t)$ is given by
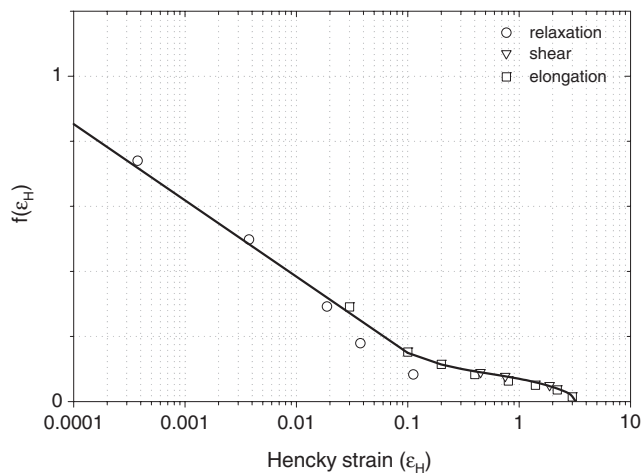
$$\tau(t) = \gamma G(1) f(\gamma) t^{-p} \qquad (15)$$

For small strains $f = 1$, and we see that the logarithmic slope of the $\tau(t)$ curve is $-p$, and $G(1)$ can also be deduced; for these samples $G'(1) = 12.2$ kPa s$^{0.27}$. Agreement with the data found from $G'(\omega)$ via Eq. 13 occurs.

We have already found $G(1)$ and p, so a plot of τ/γ against time finds $f(\gamma)$. Figure 2 shows the time response for JANZ dough for step amplitudes up to 0.3. For very small times, the rheometer response (Paar Physica MCR 300 model) is not a sudden step, and there is a delay of nearly 1 s in reaching the final strain amplitude. Details including the slow start-up are given by Tanner et al. (2007). Making allowance for this we find the damage function shown in Fig. 3. As is well known, marked softening of dough occurs even for

Fig. 2 Stress relaxation modulus (τ/γ) after initial step shear deformation for step sizes of 0.01% to 30%. The final strain (γ) is reached after $t \simeq 1$ s. The decay curves are fairly well described by power-law curves of the form $f(\gamma)G(1)t^{-p}$ for $t \gg 1$ s. The ordinate is τ/γ, the apparent shear relaxation function. The *fitted lines* all have the same form $t^{-0.27}$

Fig. 1 Showing experimental data G' and G'' for JANZ dough (*circles*) have a power-law form (*solid lines*). Here, $p = 0.27$, $G(1) = 10.7$ kPa s$^{0.27}$, $G'(1) = 12.2$ kPa s$^{0.27}$

Fig. 3 Damage function f as a function of the Hencky strain ε_H from stress relaxation measurements (*circles*), steady shearing (*inverted triangles*) and steady elongation results (*squares*). For small ε_H (<0.05), the full line shows $f = -0.0847 - 0.2344 \log \varepsilon_H$; for larger ε_H values, the values for shear and elongation are shown in Fig. 7

Fig. 4 Shear stress data for JANZ dough plotted as $\boldsymbol{\tau}/\dot{\boldsymbol{\gamma}}^p$ as a function of the Hencky strain ε_H (see Eq. 30). Fracture occurs at $\varepsilon_H \sim 3+$; $p = 0.27$. The *mean line* through the data shown is used for damage analysis

small strains. In Fig. 3, we have used the Hencky strain, ε_H, related to γ by Eq. 33. For small strains (<0.2), we have $\varepsilon_H \sim \gamma/2$.

From Fig. 3, the data from relaxation tests only go up to about $\varepsilon_H \sim 0.15$. For larger strains, we can use suddenly started steady shearing.

3. Suddenly started steady shearing

For the shear stress response to a shear rate $\dot{\gamma}$, beginning at $t = 0$, we can use the result in Eq. 12, which shows that $\tau/\dot{\gamma}^p$ is a function of strain only.
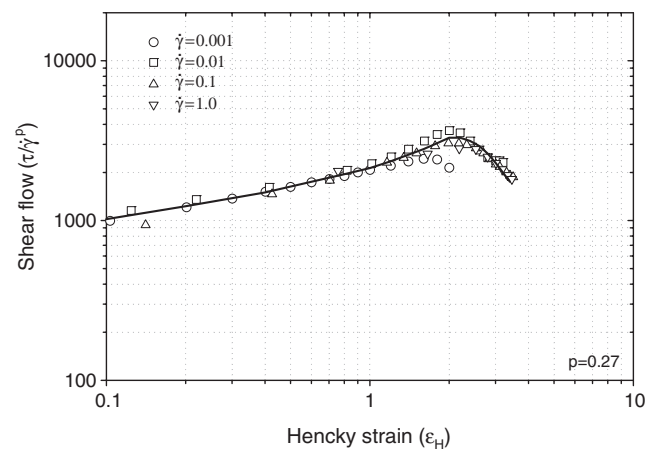
Figure 4 shows some data for JANZ dough at four shear rates ranging from 0.001 to 1.0 s^{-1}. The $\dot{\gamma}^p$ dependence is well shown. Using the solid line, the damage function $f(\varepsilon_H)$ can be found out to $\varepsilon_H \sim 3.5$, ($\gamma \sim 30$). After this the sample fractures. The values of f from shearing are plotted in Figs. 3 and 7.

Hence, we have succeeded in defining all the parameters in Eq. 1 in shear motions. It remains to be seen how the model behaves in other situations.

4. Biaxial stretching beginning at $t = 0$

We have generally followed Charalambides et al. (2002a) in doing spherical bubble-stretching experiments to deduce the stresses in biaxial deformations. We have also used almost planar deformations in "sausage" bubbles, which are nearly cylindrical.

A significant problem in our previous work (Tanner et al. 2008b) was the response in biaxial stretching.

Using the model Eq. 1 with $a = 0$ (Eq. 7) as in our previous work, the predicted stresses were only about 50% of the measured values (Fig. 5). In the previous paper, we used a complex damage function to fit the biaxial data, but paradoxically, the complex damage function eventually increased with biaxial strain, which is not satisfactory. The introduction of the **C**-term in the strain improves matters, as was found by Charalambides et al. (2002b). If we assume $a = 0.038$ in Eq. 7, the agreement is satisfactory (Fig. 5). No change in the damage function f found above is needed. Hence, we prefer this solution to our previous one. [We have also
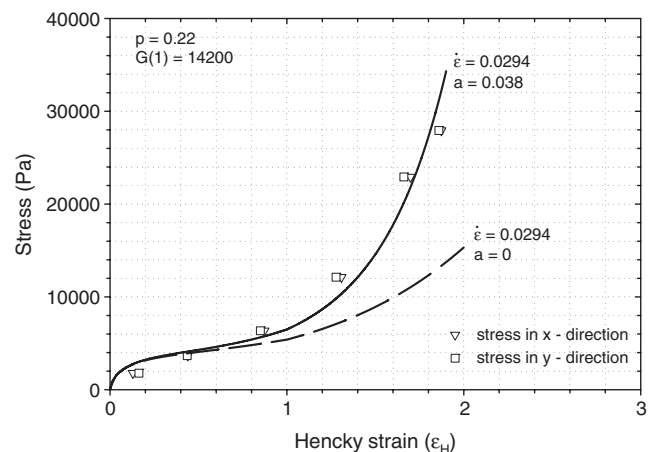
Fig. 5 Effect of changing the strain tensor from the Finger tensor to $(\mathbf{C}^{-1} - a\mathbf{C})/(1 + a)$ on biaxial stress ($\mathbf{C}^{-1}$ is the Finger strain tensor, $\mathbf{C}$ is the Cauchy–Green tensor). Here, $a = 0.038$

done squeeze-film tests which are formally equivalent to biaxial stretching. However, the maximum stretches there ($\varepsilon_H \sim 0.85$) are less than in the bubble experiments and so the effect of the **C**-term (Mooney–Rivlin term) was quite small.] The "sausage" bubble tests are also well-described using the model (Tanner et al. 2008b). The "sausage" bubble film thickness is similar to that of the spherical bubbles. Hence because of the good prediction in the "sausage" bubble case, we believe that evaporation of water from the dough is not a significant factor in the hardening of dough films—the rapid hardening in the biaxial case is simply a feature of the biaxial stretching.

5. Uniaxial elongation

We now consider steady elongation at a strain rate $\dot{\varepsilon}$ beginning from rest (we note that $\dot{\varepsilon} > 0$ for elongation; in biaxial stretching $\dot{\varepsilon} < 0$). In this case we have that the axial stress σ is of the form (Tanner et al. 2008a)

$$\frac{\sigma}{\dot{\varepsilon}^p} = f(\varepsilon_H) h(\varepsilon_H) \tag{16}$$

where $\varepsilon_H = \dot{\varepsilon} t$ ($t > 0$) in this case. From our previous work (Tanner et al. 2008a), where $a = 0$, we find that for large ε_H we have, approximately

$$\frac{\sigma}{f \dot{\varepsilon}^p} \sim G(1) \varepsilon_H^{-p} (e^{2\varepsilon_H} - e^{-\varepsilon_H}). \tag{17}$$

Now for elongation the **C** tensor is of the some form as $\mathbf{C}^{-1}$ provided λ^{-1} is substituted for λ (Eqs. 27 and 28). In the present case, the stretch $\lambda = e^{\dot{\varepsilon} t} = e^{\varepsilon_H}$. Hence, the asymptotic result for the composite strain **S** can be found by subtracting a term like Eq. 17 but with negative ε_H. We find, for large strains

$$\frac{\sigma}{G(1) f \dot{\varepsilon}^p} \sim \frac{\varepsilon_H^{-p}}{1+a} \left\{ e^{2\varepsilon_H} - e^{-\varepsilon_H} - a(e^{-2\varepsilon_H} - e^{\varepsilon_H}) \right\} \tag{18}$$

Since the first term always dominates for large ε_H, the change in stress σ is only of order a from the case $a = 0$, and since $a \sim 0.038$ for JANZ dough, this is not important. (It can also be seen that if $\varepsilon_H < 0$, as in biaxial stretching, that the term $ae^{-2\varepsilon_H}$ will eventually dominate the response. This is why the introduction of the **C**-term assists in describing biaxial stretches).

The tensile tests were carried out on an Instron 5564 machine: we have previously described (Tanner et al. 2008a) the test method and the specimen geometry; the relation between the crosshead exponential movement setting and the actual measured rate of elongation deduced from diameter measurements (made using CCD
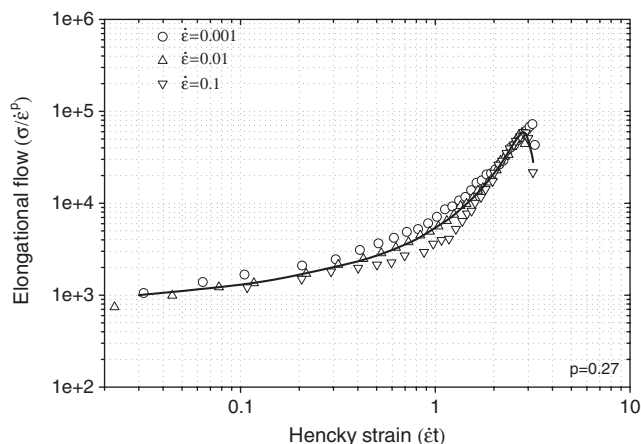
Fig. 6 Elongational stress data for JANZ dough plotted as $\sigma/\dot{\varepsilon}^p$ as a function of the Hencky strain ε_H. $p = 0.27$ here. Fracture occurs when $\varepsilon_H \sim 3.2$. The *solid mean line* is used in damage function discussions

cameras) was satisfactory, the two rates differ by only about 1%. The axial stress was obtained from the force and the measured diameter; as shown previously (Tanner et al. 2007, 2008a) the specimen cross-sections remained circular.

We show the elongational response in Fig. 6; the $\dot{\varepsilon}^p$ behaviour is evident, and the agreement of the f-function with that deduced from shearing is also clear, which is a fortunate simplification (Fig. 7). This figure compares f values deduced from elongation and shear; they are quite close, at least in the case of JANZ dough.
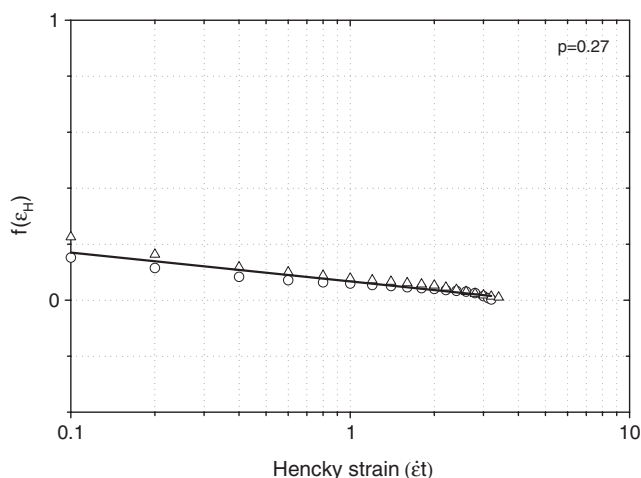
Fig. 7 Showing the damage reduction function f as a function of Hencky strain for shear and elongation of the JANZ dough. Points are experimental data; the mean curve is fitted using $f = -0.103 \log \varepsilon_H + 0.067$
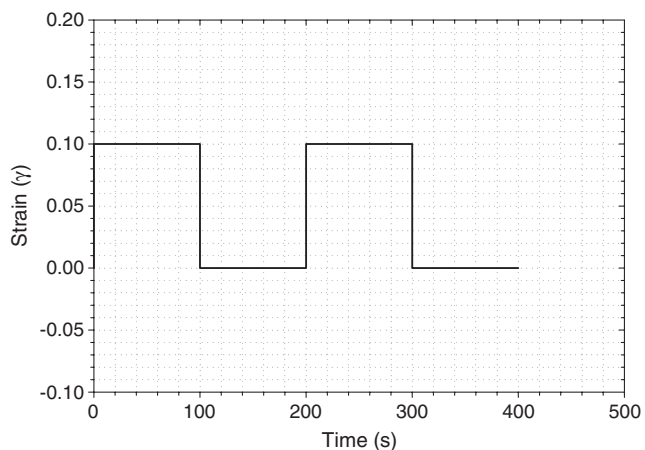
Further consideration of the damage function concept

So far, we have studied large increasing strains without reversal. Now we consider cases where reversal appears.

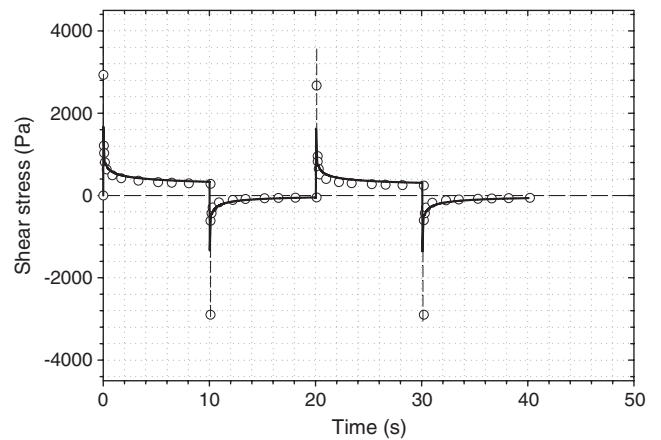### 6. Step histories of shear strain

All of the previously considered cases were for non-decreasing strains—except for the small-strain oscillatory motions where $f = 1$ in any case. We have tested the behaviour of JANZ dough in square-wave on–off shear strains (Fig. 8) with a strain amplitude of 10%. By assuming that the dough is permanently damaged by the first step of shear, the results shown in Fig. 9 are obtained. Here, the f values of Eq. 21 are used for the calculations. Whilst the agreement between the calculations and experiment is broadly good, the high measured overshoot at the step time is noticeable. We have previously attributed these experimental spikes to machine dynamics (Tanner et al. 2008b), but we will now examine the problem more closely.

The machine response for the Paar Physica MCR301 machine now needs to be considered. The actual strain found as a function of time for the first 200 ms after a 10% step command is shown in Fig. 10; there are two curves, one with a dough specimen, and the other with no specimen. The actual strains are modelled as a ramp of $\dot{\gamma}_0 = 2.5$ s^{-1} up to $t_0 = 40$ ms, followed by a constant strain (γ_0) of 0.1. Then the response can be shown to be

$$\tau(t) = \frac{G(1)}{1-p} f(\gamma)\dot{\gamma}_0 t^{1-p} \qquad (t < 0.04 \text{ s}) \qquad (19)$$

Fig. 9 Showing comparison between theory and experimental measurements for the on–off strain pattern. The calculations use the damage function of Eq. 21, and a 10-s delay time. *Symbols* are experimental measurements; the *solid line* represents calculated results with f as in Eq. 21. The overshoot values at the step change points are mainly machine artifacts
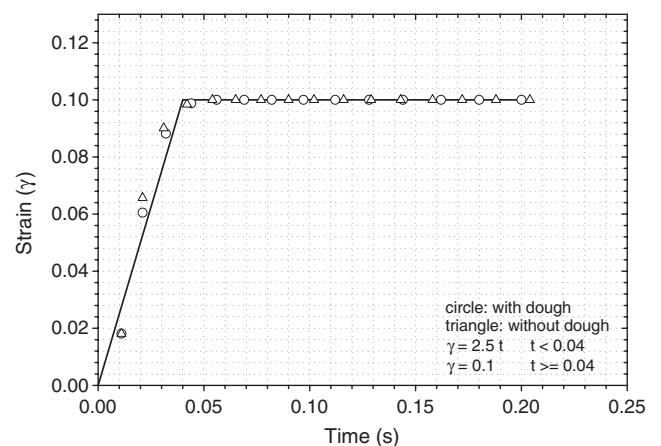
and for $t \geq 0.04$ s

$$\tau(t) = \frac{G(1)}{1-p} f(\gamma_0)\dot{\gamma}_0 \left[t^{1-p} - (t-t_0)^{1-p}\right] \qquad (20)$$

We use $\dot{\gamma}_0 = 2.5$ s^{-1}, $t_0 = 0.04$ s, $G(1) = 14.2$ kPa s^p, $p = 0.22$, and for f we use $\varepsilon_H \sim \gamma/2$ and (note: log implies a base 10 logarithm)

$$f = -0.227 \log \varepsilon_H + 0.092, \qquad (21)$$

The damage function, from Eq. 21, reaches 0.387 after 40 ms. The computed points for stress are shown in Fig. 11 as a solid line. The experimental data are shown as circles (○). Clearly for the first 20 ms, there is no

Fig. 8 Step strain (on–off) pattern. The rise and fall times are about 40 ms, so the steps are fairly steep. The strain magnitude (γ) is 0.1; and the delay between steps is 100 s


Fig. 10 Time response of rheometer to a 10% step shear command. *Symbols*: *triangles* with dough specimen; *circles* with no specimen. For the first 40 ms, there is a ramp response
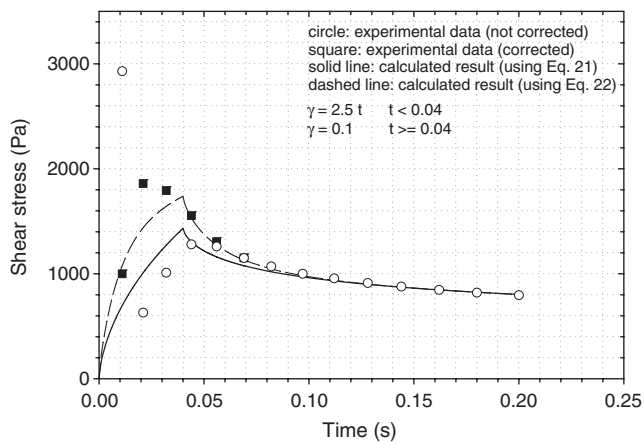
Fig. 11 Early shear stress response for JANZ dough undergoing a 10% step. *Circles* uncorrected experimental data, *squares* experimental data corrected by subtracting the false transient data of Fig. 12, *solid line* calculated result using Eq. 21, *dashed line* calculated result using f_t from Eq. 22 with the delay time $\Lambda = 0.02$ s

agreement between data and theory. A main reason is found from Fig. 12 where the machine response without a specimen is shown—there is a large inertial transient. One can subtract the apparent stress data due to inertia found from Fig. 12 to compensate for the initial transient in the first 40 ms—the results are shown in Fig. 11 (solid squares ■). There is still some divergence in Fig. 11 between the corrected data and the predictions. Some of this is probably due to the large correction needed, but it also seems possible that the simple damage function concept is inadequate for very short times. If we wish to pursue this by looking at
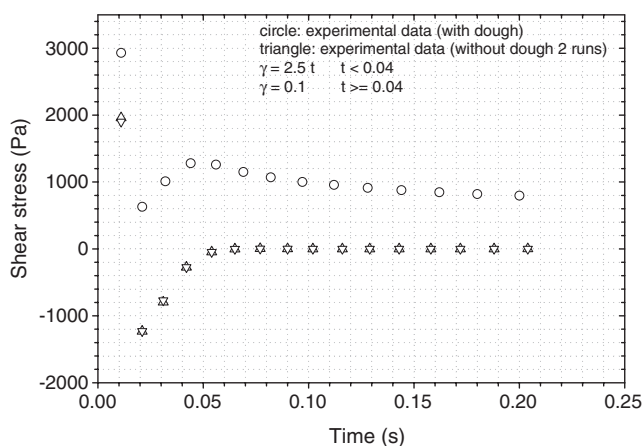
Fig. 12 Response with dough specimen (*circles*) and without dough specimen for two tests (*triangles* and *inverted triangles*). The large false inertia transient is clear
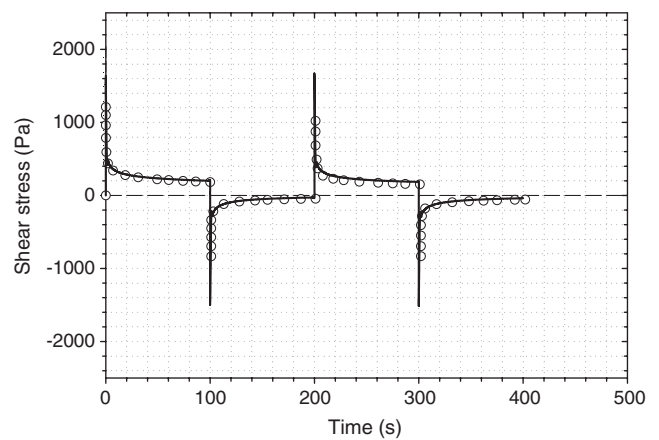

Fig. 13 As for Fig. 9, but the delay time is 100 s. Overshoots at switch times have been omitted

a 'delay' of Λ, we can use a modified time-dependent damage function:

$$f_t = f + (1 - f)e^{-t/\Lambda} \tag{22}$$

Λ is approximately 0.02 s (see Fig. 11). However, in view of the uncertainty in the inertia correction, we shall not use Eq. 22; in Figs. 13, 14, 15 and 16, we have deleted the large initial spikes.

When the reverse strain is applied, the system behaves as if it were undisturbed, and the response is a machine dynamics negative spike of magnitude 3 kPa, plus the residual stress at 10 s (0.33 kPa). The subsequent behaviour is also correctly predicted (Figs. 9, 13–16). Alteration of the dwell time from 10 to 100 s (Fig. 13) and 1,000 s shows no qualitative difference (Tanner et al. 2008b).
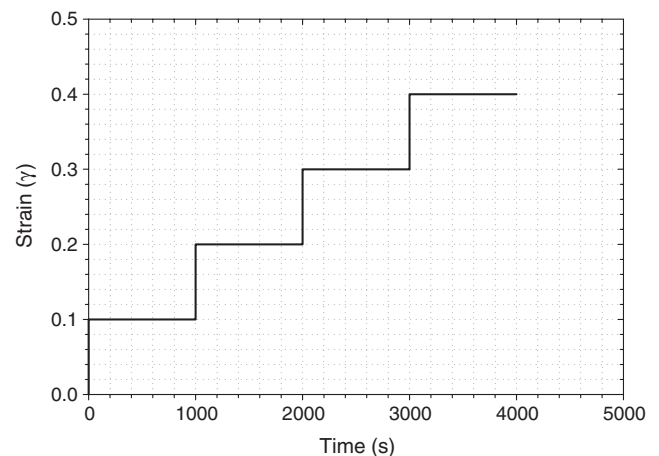
Fig. 14 'Stair case' step strain test; the delay here is 1,000 s
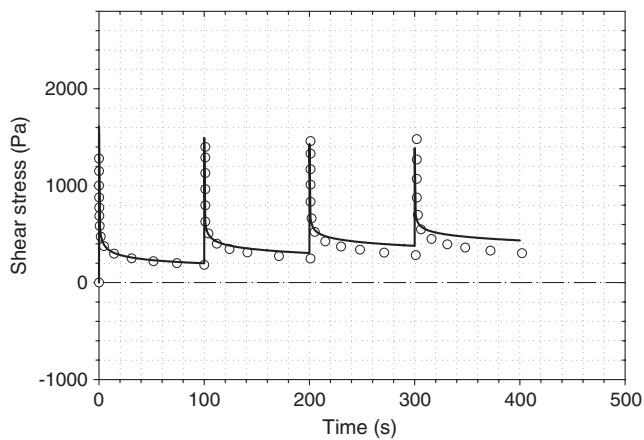
**Fig. 15** Response to stair case strain with 100 s delay. Stresses are computed using the damage function Eq. 21 which continues to decrease as the strain increases after the first step. *Symbols* are experimental measurements; the *solid line* represents calculated results. Machine artifacts for times up to 20 ms after step changes have been omitted

Similarly, for the staircase strain function (Fig. 14) the results can be correctly predicted (Fig. 15) by using Eq. 21. False spikes at each step occur as discussed above, and have been deleted. Here the damage function changes with each step. It is not accurate to assume that after the first step complete recovery occurs; if this is done the agreement with experiment is poor (Fig. 16).

The results are reminiscent of the behaviour seen by Hibberd and Wallace (1966). They subjected dough samples to a certain time of small-strain oscillation, and then a period of larger-strain oscillation, followed by a
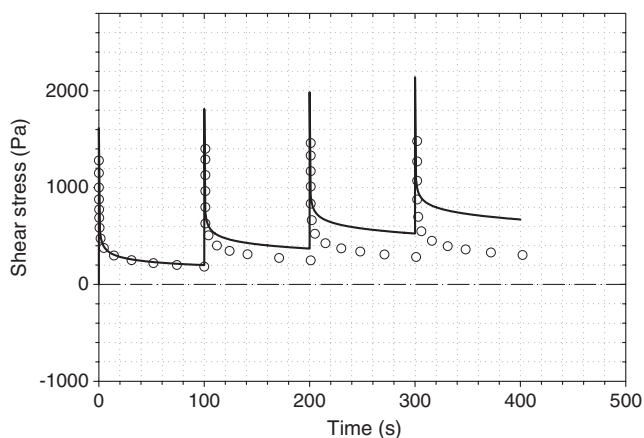
Fig. 16 As for Fig. 15, but here the damage function f is maintained at the same value ($\sim$0.387) that it acquires after the first step. The agreement with experiment is worse than in Fig. 15

return to small-strain conditions. The application of the larger strains showed an almost immediate softening, consistent with the simple damage theory, but during the subsequent small-strain period there was seen a slow, partial recovery of the moduli. Thus it appears that reversing strains, large amplitude oscillatory motion and recoil exhibit fairly complex responses, as foreshadowed in our previous work on recoil (Tanner et al. 2007).

In summary, for the step strain series experiments a picture emerges of a population of strands (f) that, after the first step of strain, supports the stress in the material, plus a population ($1 - f$) that is unstressed. When a new strain occurs, the latter part of the material responds as if it were in the virgin state, and the f–fraction also responds, but from the stressed state at $t = 10$ s. The high peaks observed are believed to be mainly machine artifacts.

Thus, we are led to behave that the damage is quasi-permanent and that the damage function f should be regarded as a function of the maximum principal Hencky strain (see Appendix A) encountered by a dough particle in its strain history; however, the participation of the unstressed strands and partial recovery of structure need to be considered in reversing flows.

7. Large amplitude sinusoidal oscillations

We have done tests at moderate strains, 0.001, 0.01, 0.05 and 0.1 (Tanner et al. 2008a) and the original damage model above would simply reduce the values of G' and G'' by a constant. The change in shape of G' and G'' with frequency is not well predicted, and the predicted magnitudes of the change at 1 Hz are not always correct. Further, if one plots the stress versus strain in the cyclic deformation, the characteristic spikes seen by Phan-Thien et al. (2000) do not appear, and the response is close to sinusoidal. To clarify this problem, we note the work of Hibberd and Wallace (1966) who subjected their dough samples to two levels of oscillatory strain at 10 Hz frequency. The results (their Fig. 2) show clearly that when the linear region ($\sim$0.1% strain amplitude) is exceeded, by the amplitude of 0.026, G' is reduced to about 0.37 of the small-strain value. In our terms, the damage function $f \sim 0.37$. (The dough used was not JANZ, but our f–function at $\gamma \sim 0.026$ ($\varepsilon_H \sim 0.013$), would be, from Eq. 21 ~ 0.52, not too different). The recovery was not complete when the level of excitation returned to the linear level but was at the 70% to 90% of that level. These observations have been repeated with our JANZ dough samples.

Hence, the oscillatory test needs to take into account the passive strands which do not bear load.

8. Recoil after stretching

In this test, the specimen is cut after elongation to a strain ε_0 and the recoil strain is computed. In a previous paper (Tanner et al. 2007), we found that it was essential to consider the non-load bearing strands, in a way similar to that outlined for step shears. We let the axial stress be σ, and the strain difference $S_{11} - S_{22}$ (elongation is along the 1 – direction) be S, finding

$$\sigma = f \int_{-\infty}^{t} m(t - t')S(t')dt' \tag{23}$$

Let the specimen be elongated for a time from zero to t_0; for $t > t_0$, $\sigma = 0$, and recoil occurs. If we consider the 'unbroken' strands, amount f, and the 'broken' strands (amount $1 - f$), we have (Tanner et al. 2007)

$$\sigma = f \int_{-\infty}^{t_0} mSdt' + f \int_{t_0}^{t} mSdt' + \beta(1 - f) \int_{t_0}^{t} mSdt'$$

$$+ \beta(1 - f)S(t_0) \int_{-\infty}^{t_0} mdt' \tag{24}$$
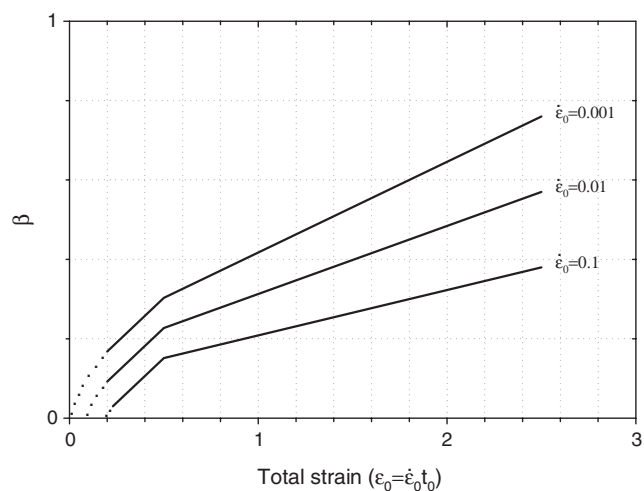
Fig. 17 The function β in Eq. 24 in terms of total strain ε_0 for various strain rates $\dot{\varepsilon}_0$. Values were deduced from experiments (Tanner et al. 2007). β goes to zero for strains less than about 0.1 as suggested by the *dotted lines*; this is in agreement with the work of Schofield and Scott Blair (1933a)
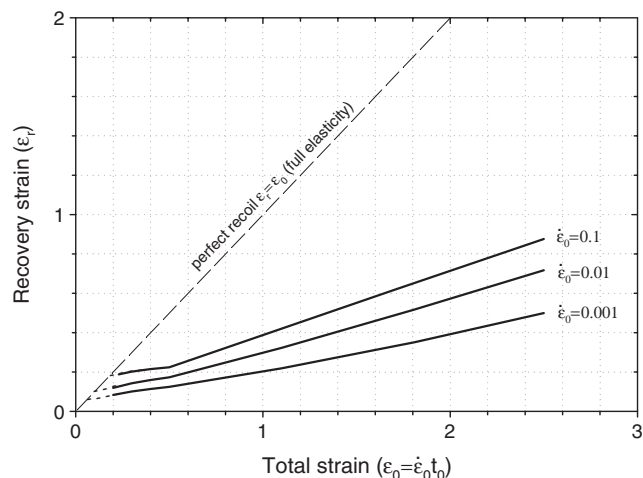
Fig. 18 The mean values of the recovery strain as a function of strain rate $\dot{\varepsilon}_0$ and total strain ε_0 applied before cutting the specimen. Note that complete recovery occurs for Hencky strains of order 0.1 and less as indicated by the *dotted lines*

We have introduced the fraction β to show what proportion of the "idle" strands participate in the backstress on recoil. If $\beta = 0$, then recoil is always complete; if $0 < \beta < 1$, incomplete recoil occurs, which is clearly more realistic in general.

For $(t > t_0)$

$$0 = f \int_{-\infty}^{t_0} mSdt' + [f + \beta(1 - f)] \int_{t_0}^{t} mSdt'$$

$$+ \beta(1 - f)S(t_0) \int_{-\infty}^{t_0} mdt'. \tag{25}$$

(Note that $\beta = 0$ if $t < t_0$). In the last term of Eqs. 24 and 25, $S(t_0)$ is constant since $t' < t_0$: and the damage function f is now also a constant, $f(\varepsilon_H) = f(\varepsilon_0)$.

We showed (Tanner et al. 2007) that it was necessary to assume β was a function of $\dot{\varepsilon}_0$ and ε_0 (Fig. 17). Thus, we were able to reproduce our recoil data (Fig. 18) and be in agreement with the pioneering work of Schofield and Scott Blair (1932, 1933a, b, 1937), who showed that recoil was complete for $\varepsilon_H \leq 0.25$. The dotted lines in Figs. 17 and 18 are suggested extrapolations consistent with their findings.

9. Creep.

In shear creep, a constant shear stress is applied and the strain is measured as a function of time. A full discussion of this case will be given elsewhere.

Conclusions

We have shown that for a wide variety of non-reversing strains (monotonically increasing strains) the simple strain-dependent damage function model of bread dough rheology is successful. The damage function reduces the stresses by a factor f, which is a function of the maximum strain encountered by a dough particle. We indicate how the parameters can be found from standard test procedures. The improved model discussed here uses a strain measure that is a linear combination of the Finger strain tensor used previously and the Cauchy–Green strain tensor. The small Cauchy–Green contribution enables us to describe uniaxial and biaxial stretching with the same damage function derived from shear data.

In the application of the model to reversing strains, we see the need to recognize the partial recovery of the microstructure after deformation and damage in order to have accurate predictions of behaviour. We consider that further work is needed in this area.

Appendix A: Strain measures used

In the concept of strain, one needs to define a reference geometry and another, the new (or strained) geometry. The deformation of the body in moving from the reference state to the new state leads to the development of the three strain forms used here ($\mathbf{C}$, $\mathbf{C}^{-1}$ and the Hencky strain ε_H). The necessary derivations for general flows can be found in Tanner (2000) and in other texts; here, we give needed results only.

The tensor $\mathbf{C}(t')$ and its inverse, $\mathbf{C}^{-1}(t')$, termed the Finger strain tensor, will be used here; it was explained by Lodge (1964) that $\mathbf{C}^{-1}$ is of major importance in describing the mechanics of rubbery materials. These tensors use the current configuration $\mathbf{x}(t)$ as the reference state; the location of a particle that is at $\mathbf{x}$ at time t, is denoted by $\mathbf{r}$ at time t', as assumed in Eqs. 3 and 4 above. Examples of the calculation of $\mathbf{C}$ and $\mathbf{C}^{-1}$ for shear are given in Eqs. 5 and 6 above. For elongation along the x-axis, lengths along the x-direction in the strained state are λ times the lengths in the reference state. Because of incompressibility, the y and z coordinates shrink by a factor $1/\sqrt{\lambda}$. Hence

$$r_x = \lambda x, \ r_y = \frac{y}{\sqrt{\lambda}}, \ r_z = \frac{z}{\sqrt{\lambda}}. \tag{26}$$

Hence, the $\mathbf{F}$ tensor is diagonal, with entries λ, $1/\sqrt{\lambda}$, $1/\sqrt{\lambda}$ for the diagonal elements, (and zero for the off-diagonal entries), so that

$$\mathbf{C} = \mathrm{diag}\left[\lambda^2, \frac{1}{\lambda}, \frac{1}{\lambda}\right] \tag{27}$$

and its inverse is

$$\mathbf{C}^{-1} = \mathrm{diag}\left[\lambda^{-2}, \lambda, \lambda\right]. \tag{28}$$

In the damage function f we use the Hencky strain magnitude ε_H as its argument. This strain is calculated from the initial rest state. Let the initial state be described by $\mathbf{X}$ (X_i in coordinate notation). Then the strain relative to $\mathbf{X}$ at time t, (the particle is now at location $\mathbf{x}$) can be written, following the equations discussed above as

$$\mathbf{C} = \mathbf{F}^T(t)\mathbf{F}(t) \tag{29}$$

where the component F_{ij} is now $\partial x_i/\partial X_j$. The Hencky strain tensor $\mathbf{H}$ is defined as

$$\mathbf{H} = \frac{1}{2}\ln \mathbf{C}. \tag{30}$$

We will use the largest principal positive eigenvalue of $\mathbf{H}$ as the measure of strain from rest (ε_H). In this Appendix, we will consider elongation and shear in detail.

In elongation, using Eq. 27

$$\mathbf{H} = \frac{1}{2}\ln\begin{bmatrix} \lambda^2 & 0 & 0 \\ 0 & \lambda^{-1} & 0 \\ 0 & 0 & \lambda^{-1} \end{bmatrix} = \begin{bmatrix} \ln\lambda & 0 & 0 \\ 0 & -\frac{1}{2}\ln\lambda & 0 \\ 0 & 0 & -\frac{1}{2}\ln\lambda \end{bmatrix}. \tag{31}$$

Since $\lambda > 1$ for elongation, the largest positive eigenvalue of $\mathbf{H}$ is $\ln\lambda$, and hence we use it as a measure of damage ε_H, where

$$\varepsilon_H = \ln\lambda. \tag{32}$$

Clearly, $\ln\lambda$ is the classical Hencky or logarithmic strain for a stretch λ (Tanner and Tanner 2003). For compression (equivalent to biaxial stretching) $\lambda < 1$, so $\ln\lambda$ is negative and the largest positive eigenvalue is now $-\frac{1}{2}\ln\lambda$.

In shear, the matter is more complex since $\mathbf{C}$ is not diagonal. However, the principal values of $\mathbf{C}$ are well known to be 1 and $1 + \frac{\gamma^2}{2} \pm |\gamma|\sqrt{1 + \frac{\gamma^2}{4}}$ (Kitoko et al. 2003). Hence, the largest positive principal strain here defines the Hencky strain in terms of γ as

$$\varepsilon_H = \frac{1}{2}\ln\left(1 + \frac{\gamma^2}{2} + |\gamma|\sqrt{1 + \frac{\gamma^2}{4}}\right). \tag{33}$$

In more complex deformations, it is generally necessary to find the largest principal strain at each point numerically.

Appendix B: Method of calculation

The value of the integral in Eq. 1 is not always easy to compute accurately, and hence we have devised an alternative method for stress computation which uses only a standard Runge–Kutta routine. The method is limited to those cases where the stress is uniform in the material, so σ is a function of time, but not of space.

We consider Eq. 1 with a single exponential memory function, so that

$$m(t) = -\frac{g_i}{\lambda_i}e^{-t/\lambda_i}. \tag{34}$$

We define

$$\tau_i = \int_{-\infty}^{t} m(t-t')\mathbf{C}^{-1}(t')dt' \tag{35}$$

and

$$\tau_i^* = \int_{-\infty}^{t} m(t-t')\mathbf{C}(t')dt'. \tag{36}$$

Then it is well known (Tanner 2000) that Eq. 35, using Eq. 34, is equivalent to

$$\lambda_i\frac{\Delta\tau_i}{\Delta t} + \tau_i = 2g_i\lambda_i\mathbf{d} \tag{37}$$

where $\mathbf{d}$ is the rate of deformation tensor, defined $d_{ij} = \frac{1}{2}(\frac{\partial v_i}{\partial x_j} + \frac{\partial v_j}{\partial x_i})$, and the upper convected derivative $\Delta\tau/\Delta t$ is given by

$$\frac{\Delta\tau_i}{\Delta t} = \frac{\partial\tau_i}{\partial t} + (\mathbf{v}\cdot\nabla)\tau_i - \tau_i\mathbf{L}^T - \mathbf{L}\tau_i \tag{38}$$

where $\mathbf{L}$ is the velocity gradient tensor, so $L_{ij} = \partial v_i/\partial x_j$. For the case when there is no spatial dependence on $\mathbf{x}$, $(\mathbf{v}\cdot\nabla)\tau_i$ is zero, and (B4) is a set of six ordinary differential equations in time for finding τ_i, which may be solved using a standard Runge–Kutta routine.

Similarly, we have for τ_i^* the lower convected derivative Maxwell model:

$$\lambda_i\left[\frac{\partial\tau_i^*}{\partial t} + (\mathbf{v}\cdot\nabla)\tau_i^* + \tau_i^*\mathbf{L} + \mathbf{L}^T\tau_i^*\right] + \tau_i^* = 2g_i\lambda_i\mathbf{d} \tag{39}$$

which also, for $(\mathbf{v}\cdot\nabla)\tau_i^* = 0$, gives a set of six ordinary differential equations in time for τ_i^*. This result can be extended to any number of relaxation times λ_i ($i = 1, 2 \cdots \cdots n$) and the sum of $\tau + a\tau*$ divided by $(1 + a)$ finds the total stresses ($\sigma + P\mathbf{I}$).

To approximate well the power-law memory function m(t) in Eq. 2 we have used 14 or 16 relaxation times (Tanner et al. 2007). These are evenly spaced logarithmically at 0.5-decade frequency, so the ratio of two successive relaxation times (λ_{i+1}/λ_i) is 3.162 ($\equiv r$).

Then from Pipkin (1986), we find

$$g_i = H(\lambda_i)\frac{r^{p/2} - r^{-p/2}}{p} \tag{40}$$

where p is the exponent in Eq. 2 and

$$H(\lambda_i) = \frac{G(1)\lambda_i^{-p}}{(p-1)!}. \tag{41}$$

Hence, there is no need for more constants—only the p and the $G(1)$ are needed to describe the complete memory function. Table 1 shows typical results for JANZ dough (We have inflated the contribution of the largest relaxation time to allow for the fact that there is no real cutoff of the spectrum).

Having these data, and initial stresses at $t = 0$ being assumed to be zero, we can solve for the stresses once the behaviour of the L_{ij} (t) components is known (in these spatially homogeneous flows, we are only interested in differences of stress, or in shear stress, so we do not have to find the pressure P). Once the τ_i and τ_i^* are found, the total stress can be found by summing over the modes $(1, 2 \cdots \cdots \cdot n)$ and multiplying by the damage function f:

$$\sigma + P\mathbf{I} = \frac{f(\varepsilon_H)}{1+a}\left[\sum_{i=1}^{n}\tau_i + a\sum_{i=1}^{n}\tau_i^*\right]. \tag{42}$$

For spatially varying flows, further work is needed; one is left to solve sets of first-order partial differential equations.

Table 1 Discrete 14-mode spectra for JANZ dough $G(1) = 14.2$ kPa s^p, $p = 0.22$

Relaxation time λ_i (s)	Modulus g_i (Pa)
0.00316	14,017.56
0.01	10,879.37
0.0316	8,446.42
0.1	6,555.47
0.316	5,089.47
1.0	3,950.06
3.16	3,066.71
10.0	2,380.15
31.6	1,847.87
100.0	1,434.18
316.2	1,113.30
1,000.0	864.18
3,162.0	670.83
10,000.0	2,326.84

The adequacy of our line spectrum can be judged from Tanner et al. (2007)

References

Abramowitz M, Stegun IA (1965) Handbook of mathematical functions. Dover, New York

Amirkaveei S, Dai SC, Newberry M, Qi F, Shahedi M, Tanner RI (2009) A comparison of the rheology of four wheat flour doughs via a damage function model. Appl Rheol 19:3 Art. 34305

Bloksma AH (1990) Dough structure, dough rheology, and baking quality. Cereal Foods World 35:237–244

Charalambides MN, Wanigasooriya L, Williams JG, Chakrabarti S (2002a) Biaxial deformation of dough using the bubble inflation technique, I. Experimental. Rheol Acta 41:532–540

Charalambides MN, Wanigasooriya L, Williams JG (2002b) Biaxial deformation of dough using the bubble inflation technique, II. Numerical modelling. Rheol Acta 41:541–545

Gabriele D, de Cindio B, D'Antona P (2001) A weak gel model for foods. Rheol Acta 40:120–127

Hibberd GE, Wallace WJ (1966) Dynamic viscoelastic behaviour of wheat flour doughs. Rheol Acta 5:193–198

Kitoko V, Keentok M, Tanner RI (2003) Study of shear and elongational flow of solidifying polypropylene melt for low deformation rates. Korea-Australia Rheology J 15:63–73

Leroy V, Pitura KM, Scanlon MG, Page JH (2010) The complex shear modulus of dough over a wide frequency range. J Non-Newton Fluid Mech 165:475–478

Lodge AS (1964) Elastic liquids. Academic, London

Ng TSK, McKinley GH (2008) Power law gels at finite strains. The nonlinear rheology of gluten gels. J Rheol 52:417-449

Phan-Thien N, Newberry M, Tanner RI (2000) Non-linear flow of a soft solid-like viscoelastic material. J Non-Newton Fluid Mech 92:67–80

Pipkin AC (1986) Lectures on viscoelasticity theory, 2nd edn. Springer, New York

Schofield RK, Scott Blair GW (1932) The relationship between viscosity, elasticity and plastic strength of soft materials as illustrated by some mechanical properties of flour doughs, I. Proc R Soc Lond A138:707–719

Schofield RK, Scott Blair GW (1933a) The relationship between viscosity, elasticity and plastic strength of soft materials as illustrated by some mechanical properties of flour doughs, II. Proc R Soc Lond A139:557–566

Schofield RK, Scott Blair GW (1933b) The relationship between viscosity, elasticity and plastic strength of soft materials as illustrated by some mechanical properties of flour doughs, III. Proc R S Lond A141:72–85

Schofield RK, Scott Blair GW (1937) The relationship between viscosity, elasticity and plastic strength of soft materials as illustrated by some mechanical properties of flour doughs, IV. Proc R Soc Lond A160:87–94

Tanner RI (2000) Engineering rheology, 2nd edn. Oxford University Press, Oxford

Tanner RI, Tanner E (2003) Heinrich Hencky: a rheological pioneer. Rheol Acta 42:93–101

Tanner RI, Dai SC, Qi F (2007) Bread dough rheology and recoil 2. Recoil and relaxation. J Non-Newton Fluid Mech 143:107–119

Tanner RI, Qi F, Dai SC (2008a) Bread dough rheology and recoil 1. Rheology. J Non-Newton Fluid Mech 148:33–40

Tanner RI, Dai SC, Qi F (2008b) Bread dough rheology in biaxial and step-shear deformation. Rheol Acta 47:739–749

Wang C, Dai SC, Tanner RI (2006) On the compressibility of bread dough. Korea-Australia Rheology J 18:127–131

Winter HH, Mours M (1997) Rheology of polymers near liquid-solid transitions. In: Neutron spin echo spectroscopy, viscoelasticity, rheology. Advances in Polymer Science, vol 134. Springer, Berlin/Heidelberg, pp 165–234